International Research Journal of Multidisciplinary Scope (IRJMS), 2026; 7(2): 1299-1309 IRJMS

Original Article | ISSN (O): 2582-631X DOI: 10.47857/irjms.2026.v07i02.08143

Graphene-reinforced Bismuth Ferrite Nanocomposites: Property Optimization

Rajata Kumar Mansingh[1], Raj Kishore Mishra[2], Tapan Dash[1,3]*, Ranjan Kumar Moharana[1], Shubhra Bajpai[4,5], Surendra Kumar Biswal[3]

[1]Department of Physics, Centurion University of Technology and Management, Odisha, India, [2]Department of Physics, Maharishi College of Natural Law, Saheed Nagar, Bhubaneswar, Odisha, India, [3]Department of R & D, International PranaGraf Mintech Research Centre (IGMRC), Bhubaneswar, Odisha, [4]Department of Pyrometallurgy & Materials Engineering, CSIR-Institute of Minerals and Materials Technology, Bhubaneswar, Odisha, India, [5]Academy of Scientific and Innovative Research, Ghaziabad, Uttar Pradesh, India. *Corresponding Author's Email: tapanphy@gmail.com

Abstract

This study investigates the graphene reinforcement in bismuth ferrite ($BiFeO_3$ or BFO) composites by powder metallurgy technique with the goal of enhancing their spectroscopic, physical and electrical properties for multifunctional applications. The powder composites prepared by dry planetary ball milling of 5 hours followed by compaction at 200 MPa and sintering at 850 ^oC for 6 hours under argon atmosphere. Results revealed a significant enhancement in the properties of composites with increasing graphene content in BFO. BFO is a promising multiferroic material; however, its practical applications are limited due to inherent drawbacks such as low electrical conductivity, rapid charge carrier recombination and limited surface area. The optimized BFO/graphene (1 mol) composite exhibited a substantial reduction (~37% reduction) in energy band gap from 2.62 eV (pure BFO) to 1.63 eV, alongside a high increase (~24-fold increase) in BET surface area from 4.9 m^2/g (BFO) to 120 m^2/g and a remarkable improvement (a four-order-of-magnitude increase) in electrical conductivity from 5.2 × 10^{-4} S/cm to 5.65 S/cm. Raman analysis indicated strong interfacial interactions and strain effects between BFO and graphene, which contribute to improved charge separation and transport. These enhancements are attributed to the synergistic effects of graphene's conductive π-network; the well-dispersed composite structure achieved via powder metallurgy and optimized processing parameters. The study concludes that 1 mol graphene-reinforced BFO is a promising candidate for next-generation applications in energy storage, photocatalysis, sensors and environmental remediation.

Keywords: Bismuth Ferrite, Graphene, Nanocomposite, Powder Metallurgy Technique.

Introduction

In recent years, the development of multifunctional materials with unique electrical, magnetic and optical properties has garnered significant attention for applications in energy, electronics and environmental remediation. Among these materials, bismuth ferrite ($BiFeO_3$ or BFO) and graphene have emerged as promising candidates due to their distinct properties. BFO is a multiferroic compound that simultaneously shows Ferro electricity and antiferromagnetism at room temperature. This unique combination permits the application of BFO in next-generation spintronics, photovoltaics and memory storage devices (1-3). Furthermore, BFO has a narrow bandgap (approximately 2.1–2.7 eV), which makes it an efficient visible-light photo catalyst (4, 5). However, pure BFO often faces challenges such as less electrical conductivity, rapid electron-hole recombination, less specific surface area, etc. which limit its practical effectiveness (6, 7). Graphene is a layer of carbon atoms that is only one atom thick, structured in a two-dimensional honeycomb lattice. It gained significant attention due to its outstanding electrical conductivity, mechanical strength, thermal conductivity and extensive specific surface area (8-10). These characteristics render it suitable for use in certain multifunctional systems which include sensors, batteries, capacitors and catalysts, among others (11-13). To improve the limitations of BFO for multifunctional applications optimized graphene reinforced BFO composites needs to be developed which integrates the multifunctional properties of BFO particularly with the high conductivity and specific surface area and structural flexibility of graphene. The incorporation of graphene into BFO can play remarkable role in improving charge transport, reduce electron-hole recombination,

(Received 10th September 2025; Accepted 06th March 2026; Published 21st April 2026)

and enhance photo catalytic efficiency of composite (14, 15). These composites will have potential stability and surface reactivity, which makes them suitable for environmental and energy-related applications. The BFO/graphene composite system holds great promise in various advanced applications, such as supercapacitors and energy storage devices, Gas and biosensors, photovoltaic devices, spintronic and magneto-electric devices, photovoltaic devices, etc. (16-19). These composites offer a synergistic effect, combining the ferroelectric and magnetic functionalities of BFO with the high conductivity and structural flexibility of graphene.

Recent research reported that rGO reinforced BFO nanocomposites synthesized through solvother-mal and sol-gel methods (20). The composites showed improved electrochemical characteristics and increased porosity, which develops charge transfer and ion diffusion in the materials, which make them as most suited ones for energy storage applications. In another study rGO reinforcement in BFO had observed to increase superior capacitance and stability in super capacitor configurations. These results are attributed to enhanced charge transport and interfacial contact between BFO and graphene sheets (21). Literature reports that rGO/BFO nanocomposites with strong photo catalytic activity under visible light have potential applications on environmental remediation due to their significant degradation of amoxicillin with remarkable recyclability (22). But the above studies face some typical limitations which includes non-uniform dispersion of graphene and its agglomeration, surface area reduction and lack of synergetic interactions, inadequately controlled in composite formation which creates difficulty in charge transfer and enhancing in electrical conductivity, etc. It has been well observed that in the conventional synthesis techniques like sol-gel, hydrothermal/ solvothermal and chemical vapour deposition (CVD), elevated temperatures or harsh chemical conditions are involved in the processing, which can produce defect in graphene part of the composites and resulting in reducing properties such as electrical and physical properties of the composites. For example, in sol-gel synthesis, we use various metal alkoxides and organic solvents, which can lead to residual carbon contamination, uncontrolled grain growth and challenges involved in restoration of graphene structure during high-temperature treatment (23). On the other hand, hydrothermal and solvothermal routes helps in achieving good crystallinity and particle size; but on the other side, they generally face non-uniform graphene dispersion, restacking of graphene sheets and limited scalability (24). These effects restrict their industrial adoptability. Due to the prolonged exposure to aqueous or chemically reactive environments, they can introduce defects in graphene and oxidation can be developed in graphene, which can cause of reduction of electrical conductivity of composites of BFO/graphene. Another method CVD is efficient for generating good quality graphene, however the method is mostly complex, costly and substrate-dependent (25). By this method, it is difficult for making bulk composite fabrication (26). Moreover, by this method, the uniform dispersion of graphene in BFO remains challenging because of the weak interfacial bonding and limited control over composite stoichiometry. However, it has been observed that the powder metallurgy approach offers a solid-state, solvent-free and effective technique for the synthesis of BFO/graphene composites (27). This method offers easy, straightforward and accurate control over the formation of the composite of BFO/graphene. Additionally, powder metallurgy minimizes chemical adverse effect on the structure of the graphene, restores in degrading graphene quality and inhibits unwanted phase transitions in BFO, which frequently occur at elevated temperatures in conventional synthesis methods. This method enables uniform dispersion of graphene in the composite. The involved mechanical milling step promotes contact between BFO phase and graphene, which helps to prevent agglomeration of graphene in the composites (27). Moreover, powder metallurgy has better control over graphene content, particle size reduction and interfacial strain, while being scalable and reproducible. Due to such advantages powder metallurgy can be considered as more effective method for producing new generation BFO/gra-phene nanocomposites. The novelty of the present work lies in the optimization of graphene reinforcement in BFO via a powder metallurgy route, enhancing superior electrical conductivity, surface area and band-gap modification via a controlled interfacial interaction, which are not

simultaneously achieved in prior studies of BFO/graphene composite (28-30).

In this work, we have taken cutting edge approach to explore and optimize the graphene reinforcement amount in BFO in view of any scope improving spectroscopic, electrical and physical properties of composite. We considered the involved challenge of the interfacial interaction between BFO and graphene, controlling morphology and dispersion of graphene sheet in composite, correlating structure, composition and adopting proper synthesis method with suitable parameters for developing optimized composites. In this work, we have prepared optimized BFO/graphene nanocomposites via powder metallurgy route under optimized parameters by varying graphene as 0.5 and 1 mol in BFO for various potential applications.

Methodology

The starting powder samples include bismuth oxide (Bi_2O_3), ferric oxide (Fe_2O_3) and graphene. Bismuth oxide has a purity of 99.9% and ferric oxide (Fe_2O_3) with a purity of 99.8%. Graphene has purity level exceeding 99.98% and having 2-4 layers of sheets. Graphene has been procured from the International PranaGraf Mintech Research Centre (IGMRC) in Bhubaneswar, Odisha, India. The graphene has been produced from high purity graphite by mechanical route. The precursor powders were mixed mechanically in an appropriate stoichiometric ratio. In this formulation, graphene was varied as 0.5 and 1 mol in BFO and the final mixture was combined with ethanol and mechanically ground in an agate mortar for approximately 3-4 hours followed by further mechanical grinding in a high-energy dry planetary ball mill under argon atmosphere for 5 hours at 300 revolutions per minute (RPM) to ensure a homogeneous blend in the composites. Tungsten carbide balls of 2 mm and 4 mm, were used as grinding media in equal quantities of 0.5 kg. A sample-to-bill ratio of 1:10 was maintained in the composite. After the milling was completed, the powder samples were extracted from the jars. Subsequently, the samples were compacted under a pressure of 200 MPa for 180 seconds in a 13 mm die. The compacted samples were then subjected to sintering in a controlled furnace within an argon atmosphere at a temperature of 850 °C for a period of 6 hours.

It has been observed that the milling time of 5 hours and a rotational speed of 300 RPM were found to be obtained as optimize conditions for ensuring effective reduction of particle size and a uniform dispersion of graphene in BFO. Beyond of these optimized conditions, excessive structural defects in the graphene may be caused. A sintering temperature of 850°C was selected to ensure complete crystallization of $BiFeO_3$ and robust interfacial bonding between BFO and graphene. The selected temperature also avoids any kind of volatilization of material. Use of argon during sintering helps to maintain the integrity of graphene and prevent undesirable phase transformations.

The features of graphene and sintered materials have been investigated through characterization methods. Particle size analysis was done via a laser scattering particle size distribution analyzer (LA-960V2, Horiba Scientific). X-ray diffraction (XRD) (PANalytical X'Pert Pro diffractometer) was used to determine the crystalline behaviour of sample. Micro Raman spectroscopy was performed using a Renishaw India Reflex (UK) spectrometer that employs an Ar+ ion laser. Brunauer-Emmett-Teller (BET) analysis was executed with an automated gas sorption analyzer from Quantachrome instruments. Field emission scanning electron microscopy (FESEM) (model ZEISS SUPRA 55) with attached energy-dispersive X-ray spectroscopy (EDS) was employed to evaluate morphological and elemental compositions of sample. Ultraviolet-Visible Diffuse Reflectance Spectroscopy (UV-Vis DRS) conducted with a Thermo Scientific Evolution 220 model. The electrical conductivity was evaluated using a four-probe digital meter (multimeter Keithley 6221). The electrical conductivity measurement for the samples was conducted at room temperature. The measured values represent the average value of five measurements. The information is incorporated in the manuscript.

Results and Discussion

The nature and quality of graphene plays vidal role in improving the property of BFO/graphene composites. The crystalline and phases structure of the graphene was studied by XRD shown in Figure 1. Various diffracted planes of carbon were identified in the XRD pattern using X'Pert HighScore software. A sharp peak is seen at around

26.4° angle which shows the presence of C (002). Some low-intensity peaks of C (011) and (110) are appeared in the graphene. No unwanted element presents in the composite.

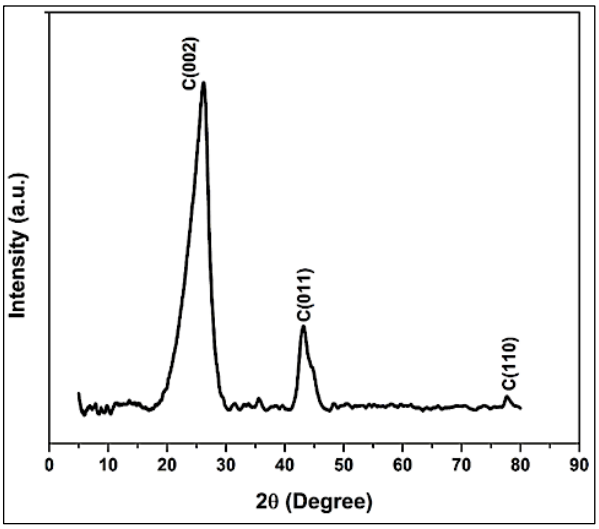

Figure 1: XRD Analysis of Graphene

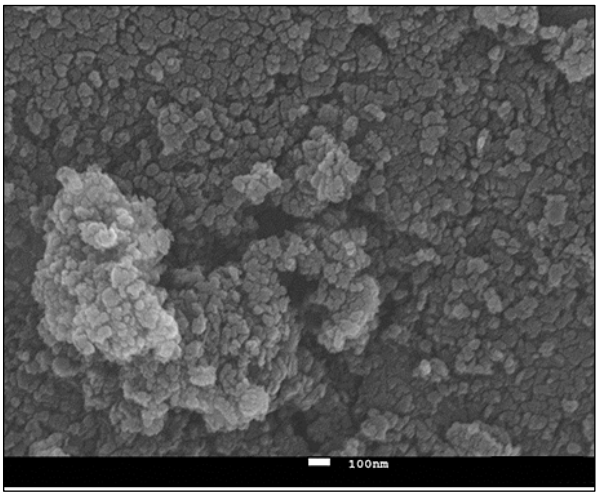

Figure 2: Morphological Analysis of Graphene using FESEM

The surface morphology of graphene has been determined by FESEM (Figure 2). It shows crumpled layers of graphene due to its flexible 2D nature. The sheets of graphene look like to be overlapped. The purity of graphene has been determined by taking EDS analysis (Figure 3) over FESEM image of graphene. It shows significant major peak for C. A trace peak for O has been detected may be due to exposure of the sample to the atmosphere. EDS analysis confirmed the absence of any unwanted elements in the graphene composite, which corroborates the XRD results showing no impurity phases. A nitrogen physisorption measurement was conducted for the graphene sample to assess the specific surface area using the BET method. The representative graph presented in Figure 4 illustrates the BET analysis (by adsorption and desorption of N_2). The BET-specific surface area was calculated to be 550.51 m^2/g. Figure 4 shows Type-I nitrogen adsorption–desorption isotherm, which infers predominant micro porosity behaviour of graphene, which can be advantageous for photo catalytic and electrochemical applications, because it promotes a large number of accessible active sites, enhances adsorption of reactant molecules and promotes efficient charge accumulation at the surface.

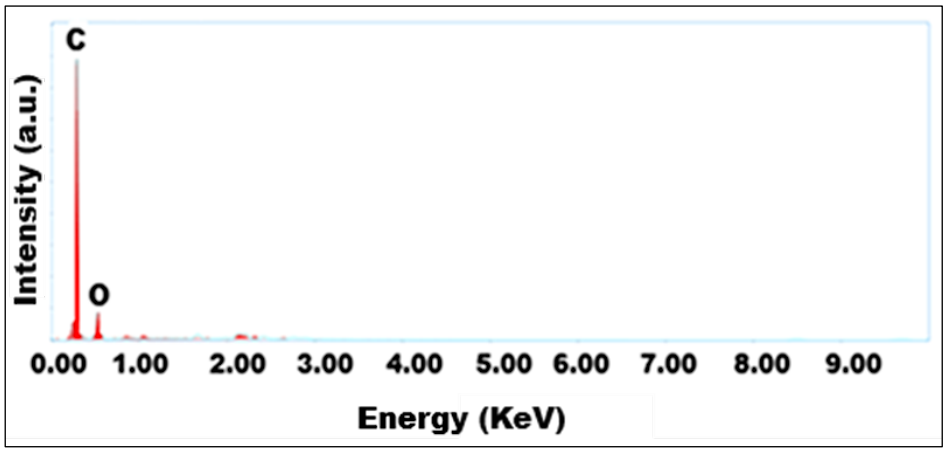

Figure 3: EDS Characterization of Graphene: Composition and Purity Assessment

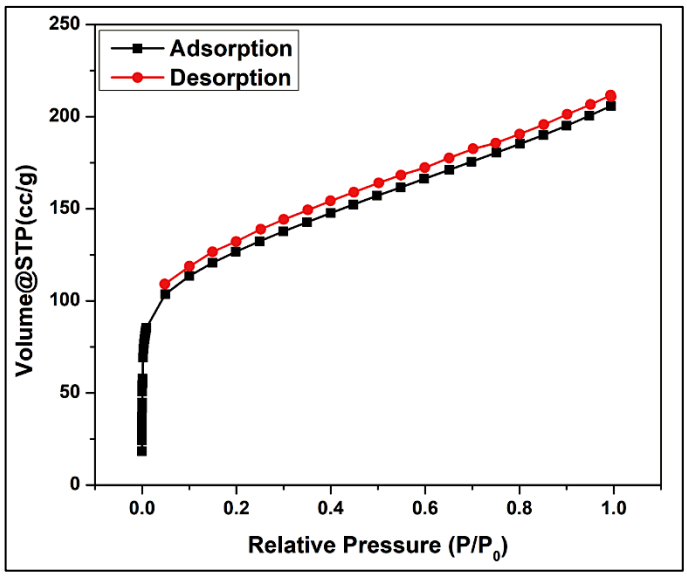

Figure 4: BET Evaluation for Determining Specific Surface Area of Graphene

Before going for sintering of the samples, the particle size after 5 hours of ball milling was determined using a laser particle size analyzer and presented in Figure 5. We had determined the median size variation (D_{50}) of BFO and BFO/graphene (0.5 mol) samples as 85 and 36 nm, respectively. These values were found to decrease as the amount of graphene increased up to 1 mol in BFO and we achieved an optimized value of particle size for the BFO/graphene (1 mol) composite at 34 nm. Consequently, the increased incorporation of graphene from 0.5 mol to 1 mol has been demonstrated to enhance the milling process, resulting in a reduction and optimization of particle size in the BFO/graphene composite. During the mechanical milling process, BFO particles become fractured and highly reactive, exposing fresh surfaces. The 2D layered structure of graphene wraps around the BFO particles, rapidly adsorbing onto these newly exposed surfaces, thus creating a physical barrier that prevents direct agglomeration. Generally, graphene considered as a solid lubricant and anti-agglomeration agent during ball milling as mentioned in the literature (31). The layered structure and weak interlayer bonding present in the graphene generate interlayer sliding and reduce friction between particles and milling media, which can cause in enhancing fracture over cold welding. The interaction between graphene and BFO can also induce localized stress and defect sites, which increases the brittleness of BFO particles, making them easier to fracture.

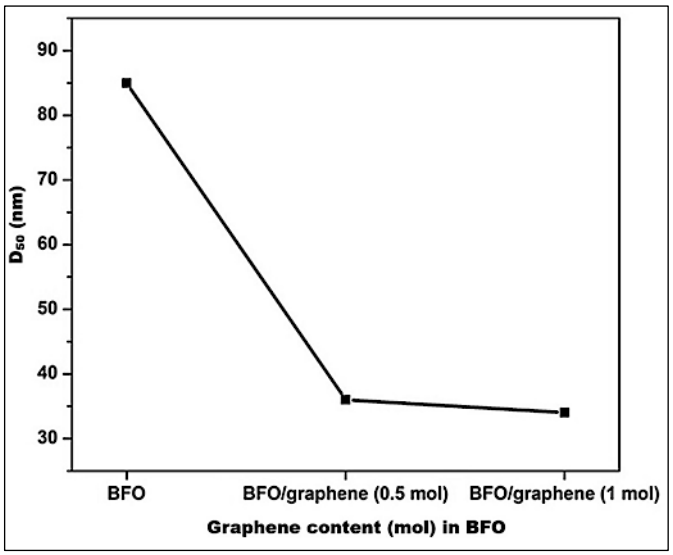

Figure 5: The Variation of the Average Particle Size (D_{50}) of BFO and the Composite of BFO/Graphene (0.5 and 1 mol)

The micro Raman spectroscopy data for the BFO and BFO/graphene composite (0.5 and 1 mol) is shown in Figure 6. BFO displays peaks at 73, 261, 311, 515, 623, 821 and 1307 cm^{-1} and such findings have been similar to the results reported in the literature (32, 33). The graphene-reinforced BFO (0.5 and 1 mol) nanocomposites show peaks for both BFO and graphene. The intensity of the peaks related to BFO decreases after the reinforcement with graphene. The peaks of graphene in the composites have been identified following to the literature (34, 35). BFO/graphene (0.5 mol) shows peaks of graphene as D (which is linked to the first disorder peak of graphite), G (which arises from sp^2 carbon within the graphite lattice) and 2D (associated with the stacking layers of graphene) at 1349, 1576 and 2695 cm^{-1}, respectively. Peaks of BFO are appeared at 73, 261, 315, 518, 625, 826 and 1309 cm^{-1}. For BFO/graphene (1 mol) composite D, G and 2D peaks observed at 1348, 1574 and 2691 cm^{-1} respectively. BFO peaks are found at Raman shift of 73, 262, 322, 434, 522, 627, 828 and 1312 cm^{-1}. The peaks associated with graphene show increase of peak intensity as the graphene reinforcement increases from 0.5 to 1 mol in BFO. Remarkably, it has been observed that on reinforcement of graphene and increasing their amount in the composite from 0.5 to 1 mol, while the peaks of BFO are slightly shifting to higher Raman shifts (except at 73 cm^{-1}), the peaks of graphene are shifting to lower Raman shifts. This type of spectroscopic behavior may be caused due to effective lattice interactions between BFO and graphene. The interaction of the lattice may also arise from the interactions between the π-electrons of graphene and the 3d orbitals of BFO, potentially resulting in charge transfer. Additionally, there might be electrostatic interactions or weak chemisorption occurring between the functional groups of C–OH in graphene and the surface atoms of BFO. The shift of BFO peaks towards higher Raman shifts indicates the existence of compressive strain within the BFO lattice, likely induced by lattice mismatch or strong interfacial bonding with graphene. Conversely, the downshift of the Raman peaks of graphene suggests the presence of tensile strain, as well as possible charge transfer between BFO and graphene, which can alter the phonon energy levels of the material. These strong interfacial interactions not only affect vibrational behavior but also enhance the electronic coupling and charge transport within the composite. The intensity ratio of the 2D band to the G band in both composites is about 0.7. The position of the 2D peak is noted to appear at a relatively lower Raman shift.

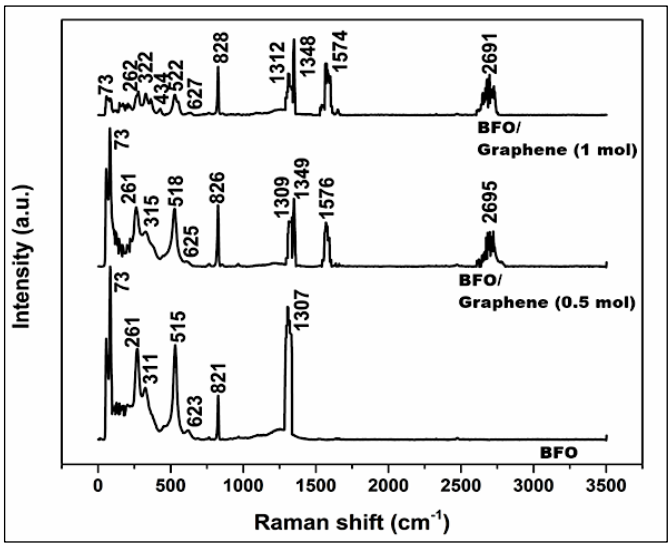

Figure 6: Micro Raman Analysis Findings of BFO and the Composite of BFO/graphene (0.5 mol and 1 mol)

The intensity and position of the 2D peak indicate that the graphene consists of 2-4 graphene sheets (36, 37). This property of graphene can significantly influence the graphene-reinforced BFO composite. As a result, the BFO/graphene hybrid composite with enhanced charge transport, interfacial bonding and strain distribution with taking benefit from graphene's high electrical conductivity and large surface area to exhibit improved electrical conductivity, charge separation efficiency and interfacial polarization, making it a promising material for advanced applications in photocatalysis, sensors and energy storage.

The energy band gap of samples was measured using the Kubelka–Munk function and presented in Figure 7 (38). As we know the composite with reduced energy band gap is crucial for improving the spectroscopic behaviour of BFO, particularly in preparing the composite for super capacitor applications. BFO shows energy band gap of 2.62 eV. On the other hand, when 0.5 mol graphene reinforced with BFO, the band gap reduced to 1.65 eV. The incorporation of graphene upto 1 mol in BFO observed to significantly further decrease and having optimize value of the band gap energy of 1.63 eV for the BFO/graphene (1 mol) composite. It is a significant achievement in the study and found to be lower than the value reported in the literature (39).

The achieved result makes a significant advancement in BFO/graphene composite research. Graphene acts as a conductive framework, creating localized states in the band structure of BFO. The potential interaction at the interface between BFO nanoparticles and graphene sheets promotes charge transfer, thereby effectively reducing the band gap. The π-conjugated system of graphene allows for the delocalization of electrons, which modifies the electronic structure of the composite. BET surface area of graphene and BFO was determined as 550.51 m^2/g and 4.9 m^2/g respectively. The incorporation of graphene of 0.5 and 1 mol reinforcement in BFO has been shown to elevate the optimized specific surface area to 112 and 120 m^2/g respectively, which is notably higher. The result is also found significantly better than the value reported in the literature (40). The electrical conductivity of BFO is about 5.2×10^{-4} S/cm. We found electrical conductivity of BFO with 0.5 and 1 mol graphene of 5.1 and 5.65 S/cm respectively. The observed enhancement in electrical conductivity for typical BFO/graphene (1 mol) composite is considerably greater than that of BFO/RGO (reduced graphene oxide) (10-30 % RGO) composites, which exhibited electrical conductivity values ranging from 4.96×10^{-2} to 1.78 S/cm (41). Similarly, our achieved electrical conductivity value is found better than the values measured for BFO/graphene composites that are already reported in literature (42).

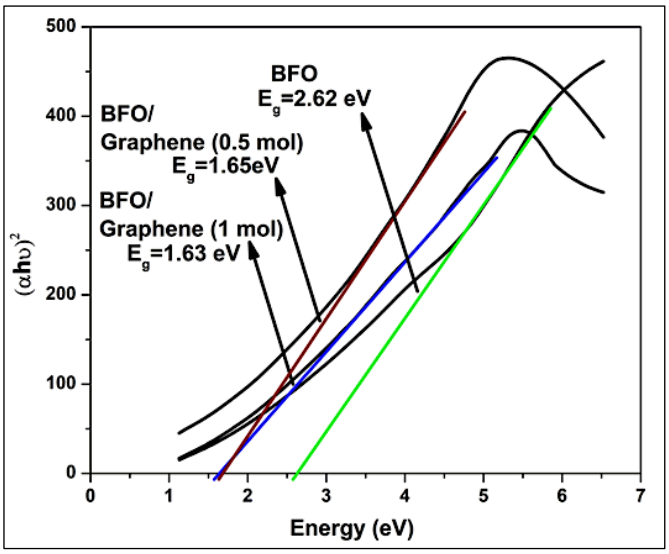

Figure 7: Results of UV-visible DRS Analysis for BFO and the BFO/Graphene (0.5 and 1 mol) Composite

The synthesis technique, specifically powder metallurgy with optimized parameter of milling (5 hours), compaction (at 200 MPa) and sintering (850^{o}C), along with the perfect graphene BFO interface, contributes synergistically to the achievement of increasing both BET SA (120 m^2/g) and electrical conductivity (5.65 S/cm) for BFO/graphene (1 mol) composite. The efficient powder metallurgy approach encourages a uniform distribution of graphene with suitable optimized amount of reinforcement (1 mol) within the BFO matrix, which in turn establishes well-connected conductive pathways throughout the composite. The π-electron configuration of graphene (0.5 and 1 mol) facilitates a more rapid charge transfer medium. Additionally, the extensive surface area of graphene enhances interfacial adhesion to BFO particles. The composite with above discussed properties make the material ready for potential work to directly evaluate the composite's performance with relatively higher scale in super capacitor and photo catalytic applications, which is our future scope of work.

Conclusion

In this study, graphene-reinforced bismuth ferrite (BFO) nanocomposites were effectively synthesized using an optimized powder metallurgy technique. Graphene was added in amounts of 0.5 and 1 mol in BFO. The mixture was combined with ethanol and ground mechanically in an agate mortar for 3-4 hours, followed by further grinding in a ball mill (tungsten carbide balls used as grinding media) for 5 hours at 300 RPM under argon. After successful formation of powder composites, the samples were compacted at 200 MPa for 180 seconds followed by sintering in an argon atmosphere at 850 °C for 6 hours. It has been observed that the incorporation of graphene significantly enhances the physical, electrical and spectroscopic properties of the BFO matrix. In particular, increasing the graphene content from 0.5 mol to 1 mol in BFO resulted in reduction in particle size (down to 34 nm), increased specific surface area (up to 120 m^2/g), enhanced electrical conductivity (5.65 S/cm) and a decrease in energy band gap (from 2.62 eV to 1.63 eV). Micro Raman and UV-Visible DRS spectroscopic analyses confirmed strong interfacial interactions between BFO and graphene, resulting in improved charge transport and better strain distribution across the composite. These achievements in the composite are attributed to the synergistic effects of graphene's high conductivity, layered structure and large surface area with the multifunctional properties of BFO. Hence, the 1 mol graphene reinforced BFO optimized composite showed significant enhancement of BFO properties, as evidenced by a 60 % reduction in particle size (D50), a ~24-fold increase in BET surface area, a four-order-of-magnitude increase in electrical conductivity and exhibited a substantial reduction (~37% reduction) in energy band gap compared to pure BFO. The results BFO/graphene nanocomposites can be inferred to consider the typical BFO/graphene (1 mol) nanocomposite as promising candidate material for advanced applications in supercapacitors, photo catalysis, sensors and energy storage systems. Future work will be

concentrated on evaluating the composite's performance in multifunctional energy and environmental technologies.

Abbreviations

None.

Acknowledgment

We extend my heartfelt gratitude to the Centurion University of Technology and Management, Odisha, India; International PranaGraf Mintech Research Centre (IGMRC), Bhubaneswar, Odisha; Maharishi College of Natural Law, Saheed Nagar, Bhubaneswar, Odisha, India; CSIR-Institute of Minerals and Materials Technology, Bhubaneswar, Odisha, India

Author Contributions

Rajata Kumar Mansingh: material preparation, data collection, analysis, interpretation of data and drafted the original work, Raj Kishore Mishra: conceptualization, study design, data collection, analysis, interpretation of data, validation, Tapan Dash: conceptualization, study design, data collection, analysis, interpretation of data, validation, Ranjan Kumar Moharana: data collection, analysis, interpretation of data, Shubhra Bajpai: data collection, analysis, interpretation of data, Surendra Kumar Biswal: resources, supervision, validation.

Conflict of Interest

The authors of this work state that they have no conflicts of interest about its publication. Ethics approval not applicable.

Data Availability

All data generated or analysed during this study are available from the corresponding author on a reasonable request.

Declaration of Artificial Intelligence (AI) Assistance

This manuscript has been developed without the use of generative AI or AI-assisted technologies. All content, research and analysis were completed manually by the author, ensuring the integrity and originality of the work.

Ethics Approval

No ethical clearance certificate is applicable for present study. The authors of the submitted paper did not receive support from any organization.

Funding

No specific grant from a government, public, private, or non-profit organization was obtained for this study.

References

1. Catalan G, Scott JF. Physics and applications of bismuth ferrite. Advanced Materials. 2009;21(24): 2463–2485. doi:10.1002/adma.200802849
2. Kharbanda S, Dhanda N, Sun AC, Thakur A. Multiferroic perovskite bismuth ferrite nanostructures: Synthesis and applications review. Journal of Magnetism and Magnetic Materials. 2023;572: 170569. doi:10.1016/j.jmmm.2023.170569
3. Zak AK, Hashim AM. Recent advances in $BiFeO_3$-based nanostructures: Properties and applications. Coordination Chemistry Reviews. 2025;523(2):1-22. https://doi.org/10.1016/j.ccr.2024.216297
4. Wang L, Hu TY, Hui K, Wang YF, Zeng JH. Enhance the photovoltaic performance via Mn-doping and interface engineering in bismuth ferrite-based ferroelectric films. Ceramics International. 2025; 51(28), 58279-58286. https://doi.org/10.1016/j.ceramint.2025.10.047.
5. Haruna A, Abdulkadir I, Idris S O. Photocatalytic activity and doping effects of $BiFeO_3$ nanoparticles in model organic dyes. Heliyon. 2020; 6: 1-8. https://doi.org/10.1016/j.heliyon.2020.e03237
6. Preethi A J, Ragam M. Effect of doping in multiferroic BFO: A review. Journal of Advanced Dielectrics. 2021;11(6):2130001. https://doi.org/10.1142/S2010135X21300012
7. Si YH, Xia Y, Shang SK, Xiong XB, Zeng XR, Zhou J, Li YY. Enhanced visible light driven photocatalytic behavior of $BiFeO_3$/reduced graphene oxide composites. Nanomaterials. 2018; 8(7):526. https://doi.org/10.3390/nano8070526
8. Geim AK. Graphene: Status and prospects. Science. 2009;324(5934):1530–1534. doi: 10.1126/science.1158877
9. Yang K, Wu C, Zhang G. A state of review for graphene-based materials in preparation methods, characterization and properties. Materials Science and Engineering*:* B. 2024;310:117698. https://doi.org/10.1016/j.mseb.2024.117698
10. Abdalla A, Hussain R, Naji A, Rinoldi C. Graphene-based nanocomposites: Synthesis, mechanical properties and characterizations. Polymers. 2021;13(17):2869. doi:10.3390/polym13172869
11. Saeed M A, Abdelkader A, Alshammari Y, Valles C, Alkandary A, Graphene applications in composites, energy and water treatment, Macromolecular Materials and Engineering. 2025; 310 (4): 2400316. https://doi.org/10.1002/mame.202400316
12. Bilisik K, Akter M. Graphene nanocomposites: A review on processes, properties and applications. Journal of Industrial Textiles. 2022;51(3): 3718S-3766S. https://doi.org/10.1177/15280837211024252
13. Wang Y, Pan C, Chu W, Vipin AK, Sun L. Environmental remediation applications of

graphene and graphene oxide: Adsorption and catalysis. Nanomaterials. 2019; 9(3): 439. https://doi.org/10.3390/nano9030439
14. Li Z, Shen Y, Yang C, Lei Y, Guan Y, Lin Y, Liu D, Nan CW. Significant enhancement in the visible light photocatalytic properties of $BiFeO_3$–graphene nanohybrids. Journal of Materials Chemistry A. 2013;1(3):823–829. doi:10.1039/C2TA00141A
15. Li Z, Shen Y, Guan Y, Hu Y, Lin Y, Nan CW. Bandgap engineering and enhanced interface coupling of graphene–$BiFeO_3$ nanocomposites as efficient photocatalysts under visible light. Journal of Materials Chemistry A. 2014;2(6):1967–1973. doi:10.1039/C3TA14269H
16. Garcés-Patiño LA, Oliva J, Reyes-Montero A, Zamora J, De la Torre T. $Bi_{0.84}Sm_{0.16}FeO_3$/ Graphene composite for flexible supercapacitors and photocatalytic dye degradation. Materials Chemistry and Physics. 2025; 341:1-19. doi: 10.1016/j.matchemphys.2025.130904
17. Si YH, Xia Y, Shang SK, Xiong XB, Zeng XR, Zhou J, Li YY. Enhanced visible light-driven photocatalytic behavior of $BiFeO_3$/reduced graphene oxide composites. Nanomaterials. 2018;8(7):526. doi:10.3390/nano8070526
18. Anandaraj C, Gajendiran J, Sabarish VCB, *et al.* Exploration of synergic effect on electrochemical behaviour of graphene and MWCNT modified $BiFeO_3$-MoS_2 composites. Diamond and Related Materials. 2023;138:110390. doi:10.1016/j.diamond.2023.110390
19. Ghadage P, Shinde KP, Nadargi D, Nadargi J, Shaikh H, Alam MA, Mulla I, Tamboli MS, Park JS, Suryavanshi S. Bismuth ferrite based acetone gas sensor: evaluation of graphene oxide loading. RSC Adv. 2024;14:1367–1376. doi:10.1039/D3RA06733E
20. Shahid M, Zaib A, Mughal J, Tariq A, Waqas U, Ramay SM, Atiq S. Optimizing $BiFeO_3$ nanostructures with reduced graphene oxide for sustainable energy storage applications. Journal of Energy Storage. 2025; 132:117888. doi:10.1016/j.est.2025.117888
21. Kumar R, Saini DS, Soam A. Reduced graphene oxide modified with bismuth iron oxide nanoparticles for supercapacitor application. Discover Applied Sciences. 2025;7:1360. doi:10.1007/s42452-025-07887-1
22. Mersa L, Seid-Mohammadi A, Samarghandi MR, Khazaei M, Asgari G. Photocatalytic degradation of amoxicillin in aqueous solutions using rGO/$BiFeO_3$ nanocomposites in the presence of LED light irradiation. Scientific Reports. 2025;15:34879. doi:10.1038/s41598-025-17033-x
23. Wang X, Mao W, Wang Q, Zhu Y, Min Y, Zhang J, Yang T, Yang J, Li X, Huang W. Low-temperature fabrication of $Bi_{25}FeO_{40}$/rGO nanocomposites with efficient photocatalytic performance under visible light irradiation. RSC Advances. 2017;7: 10064-10069. doi: 10.1039/c6ra27025e
24. Zhu Y, Murali S, Cai W, Li X, Suk JW, Potts JR, Ruoff RS. Graphene and graphene oxide: Synthesis, properties and applications. Advanced Materials. 2010;22(35): 3906–3924. https://doi.org/10.1002/adma.201001068
25. Kamel MSA, Oelgemöller M, Jacob MV. Chemical vapor deposition-grown graphene transparent conducting electrode for organic photovoltaics: Advances towards scalable transfer-free synthesis. Renewable and Sustainable Energy Reviews. 2024; 203:114740. https://doi.org/10.1016/j.rser.2024.114740
26. Acharya M, Joshi CR, Gupta A. Growth of samarium-substituted epitaxial bismuth ferrite films by chemical vapor deposition. Crystal Growth & Design.2023;23(4):2065–2074. https://doi.org/10.1021/acs.cgd.2c00984
27. Dash T, Sahoo AK, Mishra RK, Palei BB. Retaining graphene structure in the synthesis of its composite with $BiFeO_3$. Materials Today: Proceedings. 2021;43:216–219. https://doi.org/10.1016/j.matpr.2020.11.641
28. Li J, Wang Y, Ling H, *et al.* Significant enhancement of the visible light photocatalytic properties in 3D $BiFeO_3$/graphene composites. Nanomaterials. 2019;9(1):65. doi:10.3390/nano9010065
29. Irfan S, Liang GX, Li F, Chen YX, Rizwan S, Jin J, Zhuanghao Z, Ping F. Effect of graphene oxide nanosheets on structural, morphological and photocatalytic activity of BiFeO3-based nanostructures. Nanomaterials. 2019; 9(9):1337. https://doi.org/10.3390/nano9091337
30. Varshney A, Chauhan S, Sharma S. Graphene Layer-Controlled Bismuth Ferrite Nanocomposites with Enhanced Bandgap Engineering and Piezophotocatalytic Activity. J Mater Chem C. 2026; Advance Article:1-12. https://doi.org/10.1039/D5TC03424H
31. Waheed S. AbuShanab, Essam B. Moustafa, E. Ghandourah, Mohammed A. Taha, Effect of graphene nanoparticles on the physical and mechanical properties of the Al2024-graphene nanocomposites fabricated by powder metallurgy. Results in Physics. 2020;19:103343. https://doi.org/10.1016/j.rinp.2020.103343.
32. Shimizu T, Era T, Taniguchi H, Fu D, Taniyama T, Itoh M. Phonon dynamics in $BiFeO_3$ studied by Raman scattering. Ferroelectrics. 2010;403(1):187–190. doi:10.1080/00150191003751422
33. Kothari D, Raghavendra Reddy V, Sathe VG, Gupta A, Banerjee A, Awasthi AM. Raman scattering study of polycrystalline magnetoelectric $BiFeO_3$. Journal of Magnetism and Magnetic Materials. 2008;320(3–4):548–552. doi:10.1016/j.jmmm.2007.07.016
34. Ferrari AC, Basko DM. Raman spectroscopy as a versatile tool for studying the properties of graphene. Nature Nanotechnology. 2013; 8: 235-246. https://doi.org/10.1038/nnano.2013.46
35. Shabi N, Telkhozhayeva M, Girshevitz O, Kaveh M, Shlimak I. In-depth investigation into defect-induced Raman lines in irradiated graphene. Surfaces and Interfaces.2024;46:103962. https://doi.org/10.1016/j.surfin.2024.103962
36. Kumar V, Kumar A, Lee DJ, Park SS. Estimation of number of graphene layers using different methods:

A focused review. Materials (Basel). 2021;14:1–22. https://doi.org/10.3390/ma14164590
37. Politano GG, Versace C. Recent advances in the Raman investigation of structural and optical properties of graphene and other two-dimensional materials. Crystals. 2023; 13(9): 1357. https://doi.org/10.3390/cryst13091357
38. Morales AE, Mora ES, Pal U. Use of diffuse reflectance spectroscopy for optical characterization of un-supported nanostructures. Revista Mexicana de Física. 2007; 53 (5), 18-22. https://www.redalyc.org/pdf/570/57028299004.pdf.
39. Ghorbani M, Sheibani S, Abdizadeh H, Golobostan-fard MR. Modified $BiFeO_3$/rGO nanocomposite by controlled synthesis to enhance adsorption and visible-light photocatalytic activity. Journal of Materials Research and Technology. 2023;22:1250–1267. https://doi.org/10.1016/j.jmrt.2022.11.184
40. Rizwan S, Fatima S. Bismuth ferrites/graphene nanoplatelets nanohybrids for efficient organic dye removal. In: Zhou Y, Dong F, Jin S, editors. Bismuth-advanced applications and defects characterization. InTechOpen. 2018:1–24. https://www.intechopen.com/chapters/60794
41. Liao J, Ye M, Han A. Synthesis and characterization of $BiFeO_3$/RGO composites for promising microwave absorption materials. Journal of Materials Science: Materials in Electronics. 2020; 31(9): 6988–6997. https://doi.org/10.1007/s10854-020-03264-3
42. Mansingh RK, Mishra RK, Dash T, Mishra A, Biswal SK. Graphene-Reinforced BiFeONew Nanocomposite for Multifunctional Applications for Future Technology. Iraqi Journal of Applied Physics.2025; 21(4): 555-558. doi: https://doi.org/10.2025/62ng4q30

How to Cite: Mansingh RK, Mishra RK, Dash T, Moharana RK, Bajpai S, Biswal SK. Graphene-reinforced Bismuth Ferrite Nanocomposites: Property Optimization. Int Res J Multidiscip Scope. 2026; 7(2): 1299-1309. DOI: 10.47857/irjms.2026.v07i02.08143